

Spatially Probed Plasmonic Photothermic Nanoheater Enhanced Hybrid Polymeric–Metallic PVDF–Ag Nanogenerator

Chi Hao Liow, Xin Lu, Chuan Fu Tan, Kwok Hoe Chan, Kaiyang Zeng, Shuzhou Li, and Ghim Wei Ho*

Surface plasmon-based photonics offers exciting opportunities to enable fine control of the site, span, and extent of mechanical harvesting. However, the interaction between plasmonic photothermic and piezoresponse still remains underexplored. Here, spatially localized and controllable piezoresponse of a hybrid self-polarized polymeric-metallic system that correlates to plasmonic light-to-heat modulation of the local strain is demonstrated. The piezoresponse is associated to the localized plasmons that serve as efficient nanoheaters leading to self-regulated strain via thermal expansion of the electroactive polymer. Moreover, the finite-difference time-domain simulation and linear thermal model also deduce the local strain to the surface plasmon heat absorption. The distinct plasmonic photothermic–piezoelectric phenomenon mediates not only localized external stimulus light response but also enhances dynamic piezoelectric energy harvesting. The present work highlights a promising surface plasmon coordinated piezoelectric response which underpins energy localization and transfer for diversified design of unique photothermic–piezotronic technology.

Exploitation of soft electroactive polymeric hybrid systems to increase energy harvesting from ambient vibration has been envisioned as flexible self-powered material promising for implementation into self-sustained miniaturized electronics.^[1–3] Piezoelectric nanogenerator that converts mechanical forces into electricity by breaking the atomic symmetry has been particularly useful for such purpose.^[4] Although inorganic piezoelectric materials such as zinc oxide (ZnO), lead zirconate titanate (PZT), and barium titanate (BaTiO₃) exhibit high piezoelectric coefficients, they are usually brittle in nature.^[4–6] In comparison to inorganic piezoelectric materials, polymer-based piezoelectric materials such as poly(vinylidene fluoride) (PVDF)


is well-suited to fabricate flexible and biocompatible nanogenerators that can sustain large strains.^[7–9] Hence, various strategies have been employed to enhance the piezoelectric response of PVDF, primarily by preferential orientation of all-trans β -phase conformation.^[1,10,11] The proposed methodologies which yield high β -phase content from the directional nanowires, however, pose scalability issues restrictive to the size of the template.^[9,12,13] To overcome this, nanoparticles (NPs) that carry surface charges can be incorporated into PVDF to promote β -phase embodiment.^[14,15] The opposite charges on the nanoparticles form an electrostatic interaction with the highly polar C–F bond of PVDF which assist the molecular chain alignment and β -phase formation.^[16–22] Taking advantage of this compelling interaction, materials such as carbon nanotubes,^[23–25] graphene-oxide,^[13,19] metal

NPs,^[16,20,21,26,27] metal salts,^[28] and ceramic NPs have been used to induce self-aligned PVDF.^[15,29,30]

Beside, metallic nanostructure is of particularly interest in enhancing piezoresponse owing to its plasmonic light absorption down to subwavelength dimension that triggers nanoheating effect to produce localized strain via thermal expansion.^[31,32] The light-to-heat conversion via nonradiative electron relaxation dynamics^[33] leads to the spontaneous temperature increment and amplification of the incident wavelength, endowing it with intense plasmonic photothermic properties.^[33,34] The average energy density of photothermic conversion can be calculated using heat power absorption

Dr. C. H. Liow, X. Lu, C. F. Tan, K. H. Chan, Prof. G. W. Ho
Department of Electrical and Computer Engineering
National University of Singapore
4 Engineering Drive 3, Singapore 117583, Singapore
E-mail: elehgw@nus.edu.sg

Prof. K. Zeng
Department of Mechanical Engineering
National University of Singapore
9 Engineering Drive 1, Singapore 117576, Singapore

 The ORCID identification number(s) for the author(s) of this article can be found under <https://doi.org/10.1002/smll.201702268>.

DOI: 10.1002/smll.201702268

Prof. S. Li
School of Materials Science and Engineering
Nanyang Technological University
50 Nanyang Avenue, Singapore 639798, Singapore

Prof. G. W. Ho
Engineering Science Programme
National University of Singapore
9 Engineering Drive 1, Singapore 117575, Singapore

Prof. G. W. Ho
Institute of Materials Research and Engineering
A*STAR (Agency for Science, Technology and Research)
3 Research Link, Singapore 117602, Singapore

equation which gives a good approximation of heat generated by the plasmonic nanoheater.^[35–37] Coupling the localized plasmonic nanoheater with soft electroactive polymeric material allows synergetic convergence of the piezoelectric with the plasmonic photothermic effects into an integral design to enable spatially controllable and enhanced mechanical energy harvesting.^[8,38,39] However, to the best of our knowledge, such plasmonic photothermic and piezoelectric interaction in energy harvesting has rarely been reported.

Herein, we spatially probe and manipulate piezoresponse of hybrid polymeric–metallic (PVDF–Ag) system that correlates to plasmonic light-to-heat modulation of the local strain. The self-polarized Ag NPs grafted with thin PVDF sheath and PVDF–Ag NPs matrix are examined using in situ piezoresponse force microscopy (PFM) under variable visible light excitation. Notably, the in situ PFM reveals not only the spatial distribution but also provides quantitative field enhancement to underpin the surface plasmon modulated piezoelectric phenomenon. The PVDF–Ag film exhibits variable piezoelectric coefficient enhancement of 43.8% under selective visible light excitation wavelength owing to the localized plasmonic photothermic effect that spontaneously regulates the local strain. Moreover, the finite-difference time-domain (FDTD) simulation and linear thermal expansion model deduce a temperature increment of 1.9 °C which is ascribed to 8.3% plasmonic heat absorption. To this end, photothermic–piezoelectric energy harvesting demonstrates significant enhancement over pristine PVDF under plasmonic resonance. This work establishes surface plasmon enhanced piezoelectric harvesting which is highly promising for flexible plasmonic photothermic-driven piezotronic technology.

The chemical configuration of PVDF used in this study is shown in Figure 1a. There exists a large dipole moment pointing from fluorine atoms to hydrogen atoms in the ferroelectric PVDF molecule chain due to the presence of a large electron affinity difference.^[40] The formation of PVDF NPs is driven by the hydrophobic interaction between the water molecules and fluorine atoms in PVDF polymer. The hydrophobic interaction is mainly an entropic effect, which disrupts the hydrogen bonds between the water molecules and the nonpolar solute.^[40,41] Due to this reason, PVDF molecules are unlikely to form hydrogen bonds with the water molecules, hence leading to self-folding of the PVDF molecule chains to form NPs which in turn reduces the surface area exposed to the water.^[40]

Hybrid PVDF–Ag NPs were synthesized by mixing pre-prepared Ag NPs into *N,N*-dimethylformamide containing PVDF molecules, followed by the addition of a hydrophilic solvent. Because of the strong dipolar characteristic of PVDF molecules, the partial positive charges of the hydrogen atoms in PVDF will form electrostatic interaction with the partial negative charges on the surface of the Ag NPs.^[1,16,42] When a polar solvent is introduced into the mixture of PVDF and Ag NPs, the PVDF chains tend to fold on the surface of Ag NPs, encapsulating the Ag NPs within the PVDF polymer chains, as illustrated in Figure 1b.

The crystallinity of the as-grown PVDF and PVDF–Ag NPs can be further enhanced by going through an annealing process at 80 °C. All the ferroelectric properties of NPs were characterized after the annealing process.^[1,43,44] The transmission electron microscopy (TEM) images in Figure 2a,b show the successful grafting of PVDF molecules on the surface of Ag NPs with varying PVDF thickness from 7 to 15 nm. Thin layers

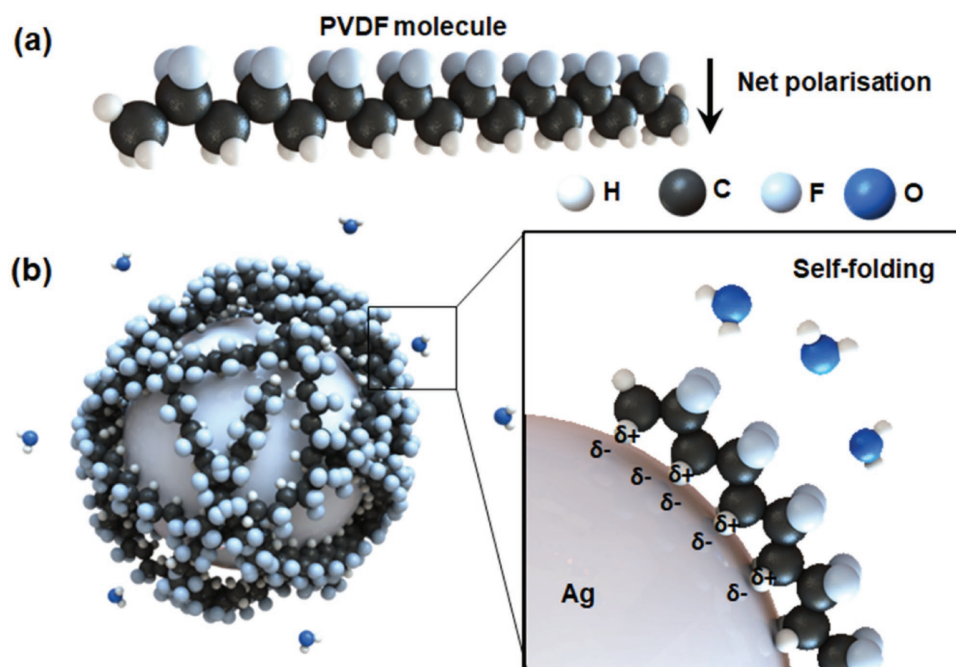


Figure 1. a) Chemical structure of PVDF in all-trans zigzag planar configuration. b) Schematic representation self-folding of PVDF molecules in β -phase configuration on the surface of Ag NPs driven by hydrophobic force. Right scheme shows the magnified image at the interface between Ag NPs and PVDF molecule via electrostatic interaction.

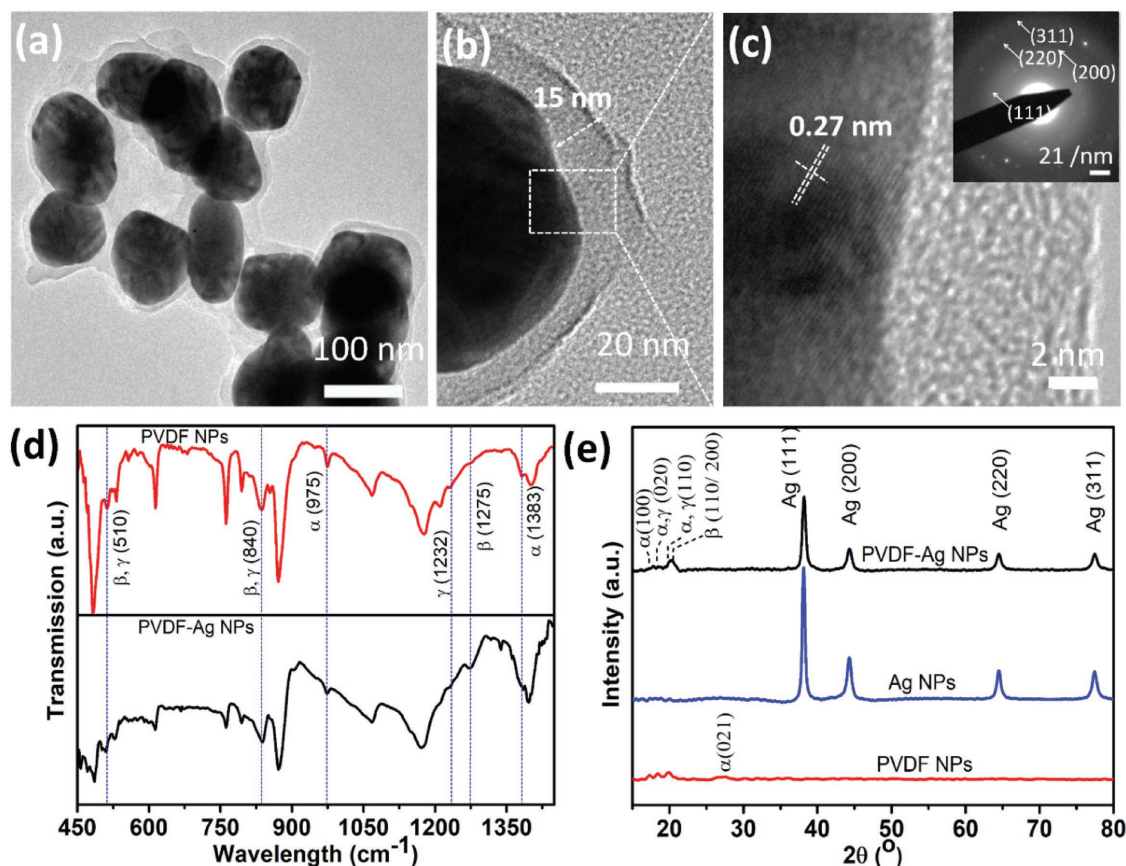


Figure 2. a,b) TEM images of PVDF–Ag NPs. c) HR-TEM image of interface at enlarged area between PVDF and Ag in PVDF–Ag NPs; the inset shows the SAED pattern of PVDF–Ag NPs. d) FTIR spectra of PVDF and PVDF–Ag NPs, e) XRD diffraction of PVDF, Ag, and PVDF–Ag NPs.

of PVDF polymer chains fold and wrap onto the surface of the nucleating site (Ag NPs), resulting in the PVDF–Ag NPs exhibiting a smaller size compared to the pristine PVDF NPs (Figure S1, Supporting Information). The interface between the Ag NPs and the PVDF grafting is shown in Figure 2c, and it is observed that the PVDF layer coats conformally onto the Ag NPs without any gaps or separation. The intimate interface between Ag NPs and PVDF suggests a strong electrostatic interaction between the electroactive PVDF β -phase and Ag NPs. The lattice fringes of the Ag NPs in the high-resolution TEM image reveal a high crystallinity structure with a d -spacing of 0.27 nm which corresponds to the (111) plane of face-centered cubic (FCC) structure. The corresponding selected-area electron diffraction (SAED) pattern is shown in the inset, and the diffraction rings are indexed to (111), (200), (220), and (311). It is noted that the intensity of the rings appear dimmer compared to pristine Ag NPs (Figure S2, Supporting Information), due to the presence of PVDF which exhibits amorphous properties in nature.^[45] The PVDF phases were identified using both Fourier transform infrared (FTIR) spectroscopy and X-ray diffraction (XRD) (Figure 2d,e). The FTIR spectrum of 450–1450 cm^{-1} is shown in Figure 2d. The electroactive β -phase can be identified from 510, 840, and 1275 cm^{-1} vibrational bands. The 510 and 840 cm^{-1} peaks are the dual signature of β and γ phases.^[46] However, with the presence of the Ag NPs, the 1275 cm^{-1} that is exclusively attributed to β -phase vibrational bands can be

clearly seen. Next, the XRD was carried out to confirm the presence of β -phase in Figure 2e. For clarity, XRD diffractogram in the range of $2\theta \approx 15^\circ$ to 24° of PVDF–Ag NPs was magnified and deconvoluted (Figure S3, Supporting Information). The presence of β phase (110/200) at 20.5° and γ phase (110) at 20.0° can be distinctively identified.^[21,47,48] The enhanced β -phase in the hybrid structure is a result of the PVDF polymer chain alignment on Ag NPs surface. Four strong Bragg reflections identified at 38.1° , 44.3° , 64.4° , and 77.4° corresponding to the Ag FCC structure^[49] are also observed in the Ag and PVDF–Ag NPs XRD diffraction patterns. These results verify that the presence of a nucleating agent can drastically promote the β -phase content, which is in agreement with previous findings.^[1,16,25,28,42,50]

The ferroelectricity of the pristine PVDF NPs and hybrid PVDF–Ag NPs were characterized by measuring their polarization-electric field (P - E) from -40 to 40 V at room temperature using PFM (Figure 3a). The 3D atomic force microscopy (AFM) topography of discrete PVDF NP and PVDF–Ag NP are shown in Figure 3b,c, respectively. The PVDF NP reveals profile height of ≈ 170 nm while the hybrid PVDF–Ag NP shows height of ≈ 80 nm, which corroborates with the size range observed in scanning electron microscopy. The PFM phase responses in Figure 3a (top) show clear hysteresis curve of the phase versus DC bias (V_{DC}). Both the pristine PVDF NPs and hybrid PVDF–Ag NPs exhibit sharp domain switch at $V_{\text{DC}} = 40$ V by $\approx 180^\circ$,

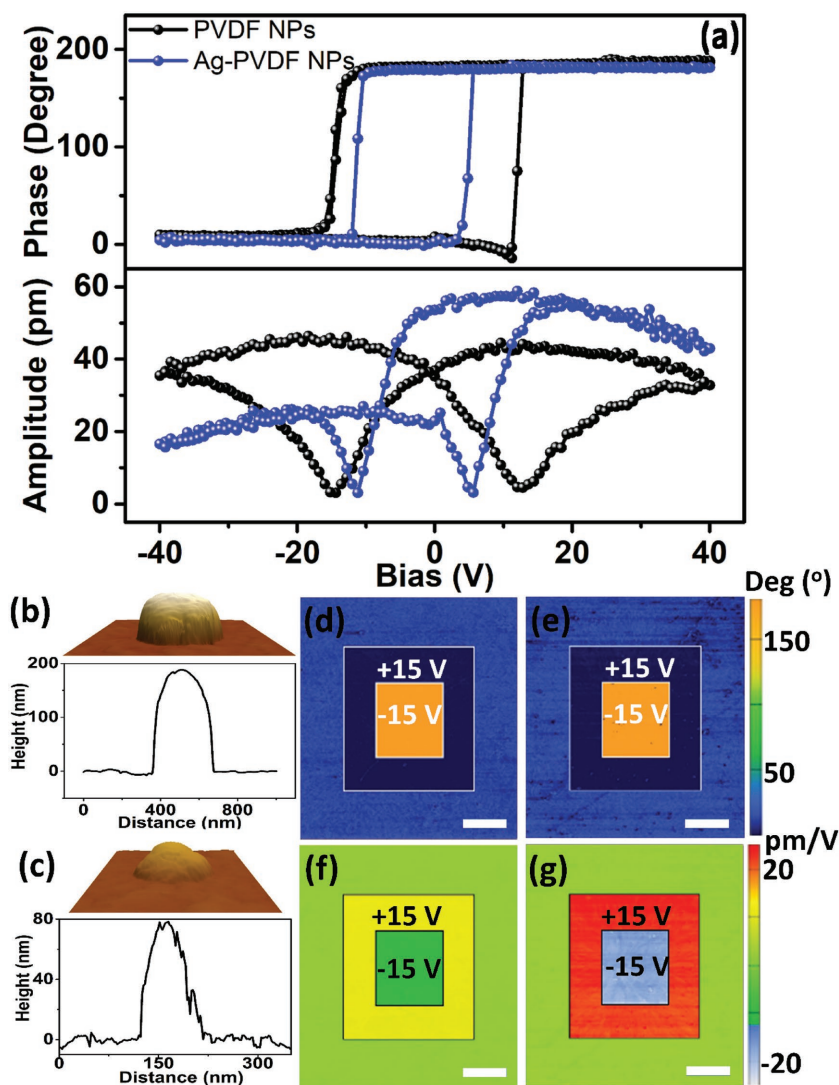


Figure 3. a) PFM measured nonlinear hysteresis loop phase (top) and amplitude (bottom) of PVDF NPs and PVDF-Ag NPs. 3D topography and height measurement of b) PVDF NPs and c) PVDF-Ag NPs. In situ blue light excitation of PFM measured polarization switching of d) PVDF film and e) PVDF-Ag film. Piezoresponse of poled f) PVDF film and g) PVDF-Ag film. Applied voltage bias is 0, +15, and -15 V based on the sequence from outer box to inner box. Scale bar is 2 μm .

with coercive voltage of $\approx \pm 13$ V (pristine PVDF NPs) and $\approx \pm 7$ V (hybrid PVDF-Ag NPs). These results suggest that a lower coercive voltage is needed to switch the PVDF domain in the presence of Ag NPs. The phase response signal is directly related to the direction of electric polarization in the microscopic region of the surface monitored under PFM tip. Hence, the 180° hysteresis switching of phase response signal to a direct-current voltage sweep is attributed to the switching of PVDF domain direction along the applied electric field, which is evident of local ferroelectricity in the pristine PVDF NPs and hybrid PVDF-Ag NPs.^[51] On the other hand, the amplitude response signal is correlated to the local strain of the PVDF experienced by the PFM cantilever. As such, expansion and contraction of the ferroelectric material upon application of an electric field results in an increased or decreased amplitude response that

resembles the “butterfly loop,” as shown in Figure 3a (bottom). It is obvious that with the presence of Ag NPs, the “butterfly loop” becomes asymmetric for PVDF-Ag NPs, which is attributed to the electrode self-poling effect arising at the interface between PVDF and Ag NPs.^[52,53] Such phenomenon facilitates upward switching of polarization but hinders downward polarization rotation in response to negative polarization.^[54] The observations of both the hysteresis phase switching and the butterfly loops validate that both PVDF NPs and PVDF-Ag NPs possess ferroelectric and piezoelectric properties.^[40,51] Different configuration systems, i.e., (i) PVDF and PVDF-Ag NPs, (ii) PVDF and PVDF-Ag NPs-film, and (iii) PVDF and PVDF-Ag film systems were studied (Figures S4 and S5, Supporting Information). Despite slight deviation between the each system, the fundamental concepts pertaining to the influence of light on the ferroelectric behavior still correlates.

PVDF films with embedded Ag NPs were prepared for further PFM studies. Figure 3d–g represents the in situ PFM measured phase and amplitude images of PVDF and PVDF-Ag films under blue light ($\lambda = 450$ nm) irradiation. The outer area of $10.0 \mu\text{m}^2$ indicates a region of unpoled PVDF and PVDF-Ag films, while the second smaller central area of $6.0 \mu\text{m}^2$ was poled by +15 V (positive polarization), and the smallest central area of $3.0 \mu\text{m}^2$ was poled by -15 (negative polarization). In the phase images shown in Figure 3d,e for both pristine PVDF and PVDF-Ag films, the unpoled, positively, and negatively polarized regions are well distinguished from one another, indicating the coexistence of both positive and negative polarization states. The corresponding amplitude signal with identical dimensions as the phase images are displayed in Figure 3f,g. Although the phase

images of both pristine PVDF and PVDF-Ag films show similar magnitudes in phase switching, the displacement observed in the PVDF-Ag film is significantly larger than that of PVDF film under the same light irradiation. In order to further investigate the tunability of the piezoresponse, light sources of different wavelengths were selectively irradiated on the PVDF-Ag films. Table 1 summarizes the PFM results of pristine PVDF and PVDF-Ag films with light (red, purple, and blue wavelengths) and without light illumination. The PFM images of red and purple light irradiations are shown in Figures S6 and S7 in the Supporting Information. The piezoelectric response of the films can be quantified by the effective piezoelectric coefficient (d_{33}) values. The d_{33} values of pristine PVDF film at +15 V without light is 11.7 pm V^{-1} and with blue light is 11.0 pm V^{-1} . These results indicate that light irradiation has insignificant

Table 1. Summary of piezoresponse of PVDF film and PVDF–Ag film under different electromagnetic wavelength illumination.

Light	Amplitude [pm]			Phase [°]			Effective piezoelectric coefficient, d_{33} [pm V ⁻¹]		
	0 V	+15 V	-15 V	0 V	+15 V	-15 V	0 V	+15 V	-15 V
Pristine PVDF film									
None	9.2	58.5	50.5	13.6	0.2	179.8	1.8	11.7	-10.1 ^{a)}
Red	9.0	56.8	48.4	12.0	0.1	179.3	1.8	11.4	-9.7
Purple	7.7	57.4	46.3	13.4	0.9	179.3	1.5	11.5	-9.3
Blue	9.0	54.8	49.8	12.8	0.5	179.3	1.8	11.0	-10.0
PVDF–Ag film									
None	8.9	79.1	67.5	18.5	0.5	179.0	1.8	15.8	-13.5
Red	12.1	74.7	68.3	19.9	1.8	180.0	2.4	14.9	-13.7
Purple	13.3	103.3	83.3	18.6	2.2	179.0	2.7	20.7	-16.7
Blue	12.4	113.3	88.3	13.3	0.2	178.8	2.5	22.7	-17.7

^{a)}The negative sign is determined by considering the film spontaneous polarization direction driven by the AC field.

influence on the piezoelectric response of the pristine PVDF. However, when Ag NPs are introduced into the PVDF film, an increment in the piezoelectric response is observed. Under blue light irradiation, the effective d_{33} of PVDF–Ag film achieved the highest piezoresponse of 22.7 pm V⁻¹, which is 43.8% higher than that without light irradiation. This piezoelectric coefficient is also 106.4% higher than that of pristine PVDF film which can be attributed to the increase of the β -phase content due to self-poling effect (Figure 3a).

In general, the effective d_{33} measured using PFM can be described by $d_{33} = X/V$, where X is the measured local displacement (amplitude) of the film and V is the drive amplitude (5 V) of the cantilever.^[51] Without light irradiation, the amplitude of the PVDF–Ag film yields 79.1 and 67.5 pm under +15 and -15 V voltage biases. In the presence of 450 nm light illumination, the local displacement of the same film at voltage biases of +15 and -15 V increased to 113.3 and 88.3 pm, respectively. Comparing the displacement obtained with and without 450 nm light irradiation, the local strains are estimated to have increased by 43.2% and 30.8% at +15 and -15 V voltage bias, respectively. These results indicate that the PVDF–Ag film effectively responded to specific light irradiation wavelength and the plasmonic photothermic effect induced an additional local strain enhancement, which causes, the effective d_{33} values to be greatly enhanced. Since the local strain is linearly proportional to the displacement of the piezoelectric material,^[51,55] one can expect an intuitive inclusion of the additional local strain of PVDF–Ag in the presence of light which can be represented by $d_{33} = (X + X_{Ag})/V$, where X_{Ag} is the additional local strain.

To explain the light-driven additional local strain, X_{Ag} , observed in the PVDF–Ag film, the thermal expansion model of a polymer was adapted as illustrated in Figure 4a. Upon light excitation, the electron will be excited to a higher energy state which subsequently relaxes by electron–electron scattering. The fast heating results in cooling equilibrated by electron–phonon relaxation. Finally, the phonon energy is dissipated to the surrounding environment.^[56] The heat dissipated from the nanoheater results in thermal expansion of the PVDF film. Notably, during the PFM measurement, the temperature of the measuring platform was assumed to be constant. Hence, the heat

that induces the film expansion can be assumed to originate solely from the Ag NPs under blue light irradiation. It is proposed that under the “optimal” incident wavelength, the plasmonic resonance is excited and converts light into heat that eventually expands the film. It is also possible that the enhancement observed might be contributed by the pyroelectric effect of PVDF, however, pyroelectric energy can only be generated when a temperature gradient exists. In this work, the heat generated due to the light irradiation has been equilibrated with its surrounding, therefore ruling out the pyroelectric contribution due to temperature change.

In order to support the proposed mechanism, the UV–vis extinction spectra of the Ag NPs in ethanol suspension and PVDF–Ag film were measured. Figure 4b reveals a dipolar plasmon mode of Ag NPs at 440 nm and PVDF–Ag film at 450 nm.^[57] The red shift of 10 nm for the localized surface plasmon resonance (LSPR) peak can be attributed to an increase in the effective refractive index of the surrounding medium.^[58–60] Meanwhile, the pristine PVDF film shows a weak absorption in the visible spectrum because of its large bandgap. The electromagnetic properties of the Ag NPs were also studied using the FDTD method. The peak positions of the calculated extinction spectra are in good agreement with that of the measured UV–vis spectra. However, the measured dipolar plasmon mode of Ag NPs appears to be broader than the calculated one, owing to the wide particle size distribution of the as-synthesized Ag NPs.^[61] In order to further investigate the plasmonic effect on the piezoresponse enhancement, different light sources used in PFM measurement were superimposed on the extinction spectrum of PVDF–Ag film as shown in Figure 4c. The shaded regions are the overlapping areas between the light excitation sources and the LSPR of Ag NPs in PVDF–Ag film. It is obvious that the blue light illumination has the closest match with the Ag plasmonic resonance spectrum as compared to that of other light illumination wavelengths.

It is noted that the extinction spectrum might have included light scattering at different angles. Using electromagnetic simulation, power absorption is calculated to gain insight of the piezoresponse enhancement mechanism. As the power absorbed by a material depends on the divergence of the Poynting vector,

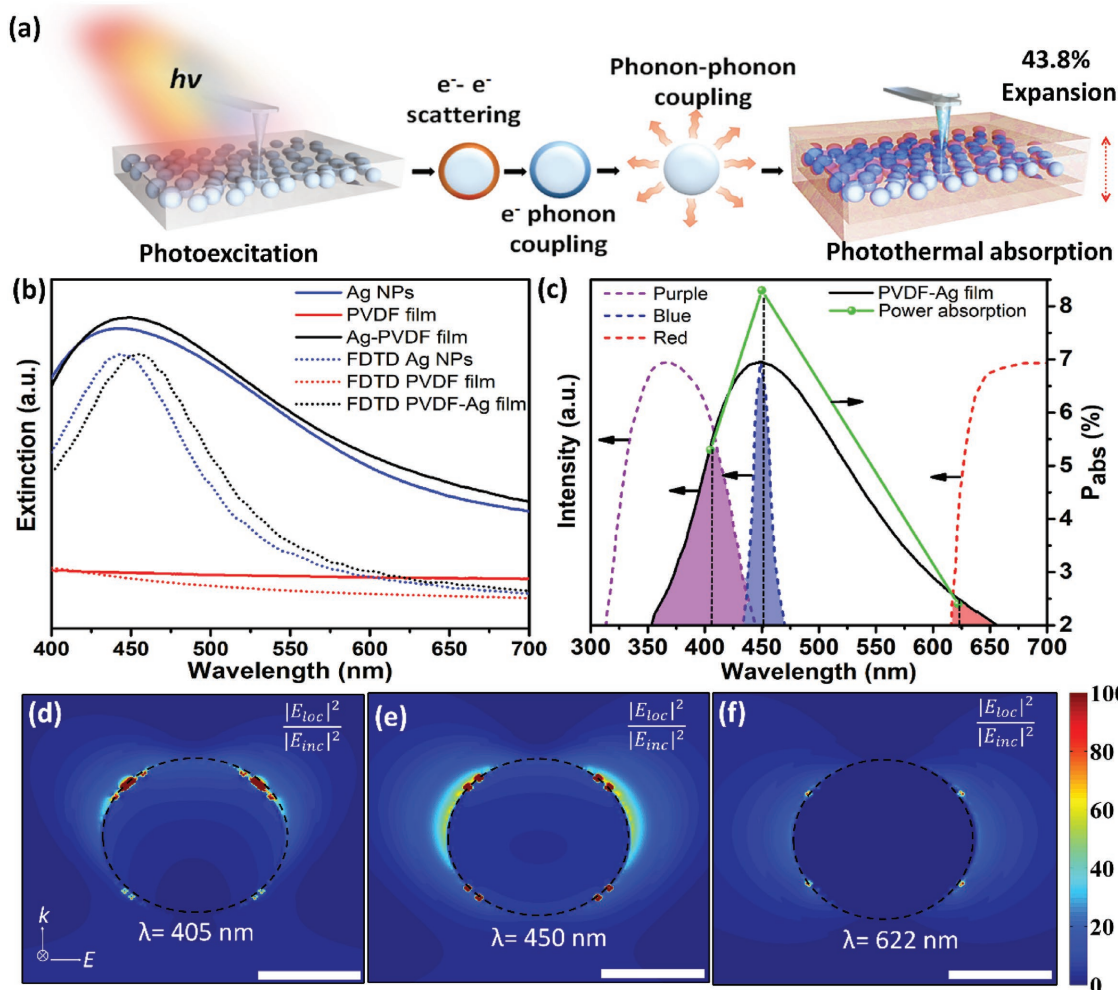


Figure 4. a) Thermal expansion model based on light to heat conversion for PVDF–Ag film. b) Numerical calculated and UV–vis measured extinction spectra of Ag NPs, PVDF, and PVDF–Ag film. c) Overlap of PVDF–Ag extinction spectra with different light bands and FDTD calculated power absorption. Numerical simulated electric field distribution of Ag NPs in PVDF film at d) 405 nm, e) 450 nm and f) 622 nm. Scale bar is 50 nm.

the absorbed heat power of nonmagnetic materials can be calculated based on the simple equation $P_{\text{abs}} = 1/2\omega\epsilon''|E|^2$, where ω is the frequency, ϵ'' is the imaginary part of the dielectric permittivity, and E is the total electric field.^[32,35] The calculated power absorption for Ag NPs in PVDF matrix at three different excitation wavelengths is illustrated by the green curve in Figure 4c, which qualitatively agrees with the LSPR peak of UV–vis spectrum. Careful examination of the overlapping area between the light illumination and the Ag NPs LSPR spectra reveals a higher power conversion (8.3%) of Ag NPs under blue light irradiation than red light irradiation (2.4%). The electric field distribution of PVDF–Ag film at three different excitation wavelengths are plotted in Figure 4d–f, showing dipolar plasmon mode for all three excitation wavelengths.

By analyzing the ability of the plasmonic nanoparticles to convert the absorbed light to heat, the mechanism behind the enhancement of the effective d_{33} value of PVDF–Ag film under different light conditions was elucidated. When the wavelength of the incident light is close to the resonance frequency of the metallic nanoparticle, more energy will be converted into

heat. The heat will then dissipate across the particle interface to the adjacent matrix medium due to phonon–phonon interaction (Figure 4a).^[62,63] Generally, polymer undergoes physical deformation when subjected to temperature changes: it expands when heated and contracts when cooled. In this study, the elastic modulus of the PVDF–Ag was assumed to remain unchanged in all the light irradiation conditions. Hence, it has inconsequential effects on the d_{33} value. Explicitly, the additional local strain of X_{Ag} can be related to the effectiveness of light to heat conversion by Ag NPs under blue light excitation. The linear thermal expansion is expressed as $\Delta d = \alpha \cdot d_i \cdot (\Delta T)$,^[64] where Δd is the change in thickness, α is the coefficient of thermal expansion of PVDF ($12.5 \times 10^{-5} \text{ m}^{-1} \text{ K}^{-1}$), d_i is the initial thickness of film (110 nm, which was obtained from AFM measurement of PVDF–Ag film in Figure S8 (Supporting Information)), and ΔT is the change in temperature. By comparing the average change in thickness at voltage biases of 0, +15, and –15 V with light irradiation to that without light irradiation, quantitative estimation of the average $\Delta T \approx 1.9$ and ≈ 0 °C, under blue and red light irradiation, respectively, can

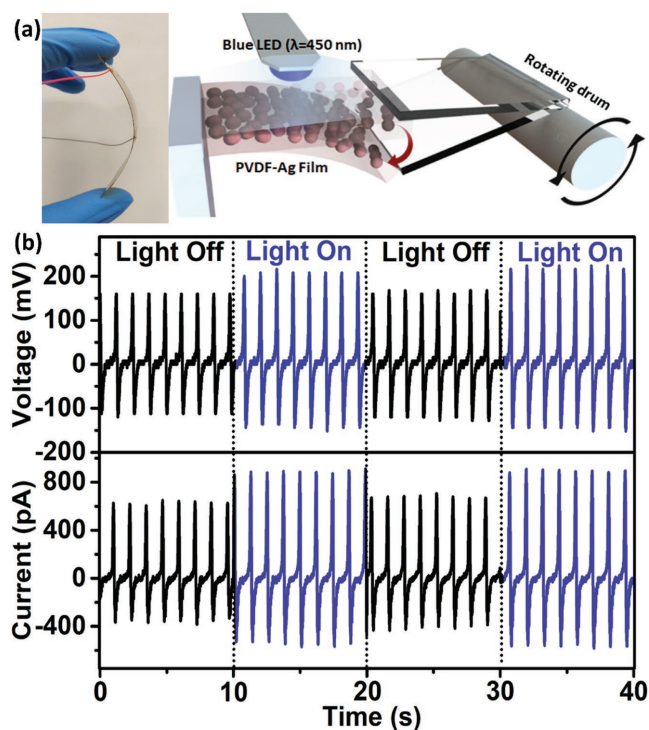


Figure 5. a) Photograph of flexible PVDF–Ag film on ITO–PET sheet and schematic of experimental setup used for light enhanced piezoelectric energy harvesting by periodic bending of the PVDF–Ag film. b) Cycling of measured open-circuit voltage and short-circuit current of the PVDF–Ag nanogenerator with and without blue light illumination.

be calculated from the linear thermal expansion model. The changes in the average temperature of the PVDF–Ag films are in good agreement with the FDTD calculated power absorption.

In order to demonstrate the energy harvesting capability under the influence of light, a flexible PVDF–Ag film coated on an ITO–PET sheet was fabricated (Figure 5a). The piezoelectric performance of the hybrid system was investigated with and without blue light ($\lambda = 450$ nm) illumination as shown in Figure 5b. Periodic bending was administered to the PVDF–Ag film via a motor driven mechanical arm of 0.8 Hz rotation, and the piezoresponse of the film as a function of time was obtained (Figure 5b). Under the dark condition, the average peak value of the open-circuit voltage and short-circuit current are 160 mV and 640 pA, respectively. When the same mechanical bending was repeated in the presence of blue light illumination, both the voltage and current output increased to 210 mV and 890 pA, respectively. The voltage and current output are enhanced by 31% and 39%, respectively, compared to that without light illumination. It is known that higher piezoelectric coefficient results in enhanced energy harvesting.^[65] From Figure 4, when the incident light is close to the resonance wavelength of the Ag nanoparticle, more heat will be dissipated across the particle interface to the adjacent matrix medium due to phonon–phonon interaction. This results in an increasing of the average temperature in the PVDF–Ag system, hence larger local displacement of the PVDF. Consequently, the photothermic effect that increases the piezoelectric coefficient of the PVDF matrix correlates to higher energy output under

blue light illumination. It is noted that a pristine PVDF film shows significantly lower voltage and current output (Figure S9, Supporting Information). Moreover, it does not respond to the cyclical on–off blue light irradiation. This demonstration verifies the effect of plasmonic nanoheater on piezoresponse which leads to enhanced energy harvesting.

In summary, we have successfully synthesized self-polarized ferroelectric hybrid polymeric–metallic PVDF–Ag and demonstrated its distinctive plasmonic photothermic–piezoelectric properties. The hybrid PVDF–Ag NPs reveal higher β -phase which significantly lower the coercive voltage needed for the piezoelectric hysteresis switching. Additionally, the PVDF–Ag shows a piezoresponse enhancement of 43.8% under resonant light irradiation at room temperature. The enhanced piezoresponse is attributed to the thermal expansion induced local strain of PVDF owing to the plasmonic photothermic effect of Ag NPs which convert light to heat in the PVDF matrix. This finding is critical to improve the performance of piezoelectric materials. Using numerical electromagnetic calculation and linear thermal expansion model, the power absorption was calculated to be 8.3%, leading to an increase in the PVDF–Ag film temperature by 1.9 °C under blue light irradiation. We successfully validated the energy harvesting functionality of a hybrid PVDF–Ag film which outperforms pristine PVDF and responds to resonant blue light illumination. This study provides an important physical insight into the interaction between the light and piezoelectric properties useful for the design and fabrication of efficient plasmonic photothermic-driven piezotronic energy harvesters.

Supporting Information

Supporting Information is available from the Wiley Online Library or from the author.

Acknowledgements

C.H.L. and X.L. contributed equally to this work. This research is supported by the Singapore Ministry of National Development and the National Research Foundation, Prime Minister's Office under the Land and Liveability National Innovation Challenge (L2 NIC) Research Programme (L2 NIC Award No. L2NICCFP2-2015-3).

Conflict of Interest

The authors declare no conflict of interest.

Keywords

photothermal, piezoelectric, plasmonic light-to-heat conversion, plasmonic resonance

Received: July 4, 2017
Revised: October 9, 2017
Published online: December 14, 2017

- [1] P. Martins, A. C. Lopes, S. Lanceros-Mendez, *Prog. Polym. Sci.* **2014**, *39*, 683.
- [2] Z. L. Wang, G. Zhu, Y. Yang, S. Wang, C. Pan, *Mater. Today* **2012**, *15*, 532.

- [3] H. D. Espinosa, R. A. Bernal, M. Minary-Jolandan, *Adv. Mater.* **2012**, *24*, 4656.
- [4] Z. L. Wang, J. H. Song, *Science* **2006**, *312*, 242.
- [5] P. K. Panda, *J. Mater. Sci.* **2009**, *44*, 5049.
- [6] W. Wu, S. Bai, M. Yuan, Y. Qin, Z. L. Wang, T. Jing, *ACS Nano* **2012**, *6*, 6231.
- [7] V. Bhavanasi, V. Kumar, K. Parida, J. Wang, P. S. Lee, *ACS Appl. Mater. Interfaces* **2016**, *8*, 521.
- [8] T. K. Sinha, S. K. Ghosh, R. Maiti, S. Jana, B. Adhikari, D. Mandal, S. K. Ray, *ACS Appl. Mater. Interfaces* **2016**, *8*, 14986.
- [9] R. A. Whiter, V. Narayan, S. Kar-Narayan, *Adv. Energy Mater.* **2014**, *4*, 1400519.
- [10] M. Nasir, H. Matsumoto, M. Minagawa, A. Tanioka, T. Danno, H. Horibe, *Polym. J.* **2007**, *39*, 670.
- [11] A. Jain, K. J. Prashanth, A. K. Sharma, A. Jain, P. N. Rashmi, *Polym. Eng. Sci.* **2015**, *55*, 1589.
- [12] Y. Calahorra, R. A. Whiter, Q. S. Jing, V. Narayan, S. Kar-Narayan, *Appl. Mater.* **2016**, *4*, 116106.
- [13] S. K. Karan, R. Bera, S. Paria, A. K. Das, S. Maiti, A. Maitra, B. B. Khatua, *Adv. Energy Mater.* **2016**, *6*, 1601016.
- [14] B. B. Jiang, X. C. Pang, B. Li, Z. Q. Lin, *J. Am. Chem. Soc.* **2015**, *137*, 11760.
- [15] M. F. Lin, P. S. Lee, *J. Mater. Chem. A* **2013**, *1*, 14455.
- [16] S. Manna, S. K. Batabyal, A. K. Nandi, *J. Phys. Chem. B* **2006**, *110*, 12318.
- [17] P. Martins, C. M. Costa, M. Benelmekki, G. Botelho, S. Lanceros-Mendez, *CrystEngComm* **2012**, *14*, 2807.
- [18] S. Garain, T. K. Sinha, P. Adhikary, K. Henkel, S. Sen, S. Ram, C. Sinha, D. Schmeisser, D. Mandal, *ACS Appl. Mater. Interfaces* **2015**, *7*, 1298.
- [19] O. D. Jayakumar, E. H. Abdelhamid, V. Kotari, B. P. Mandal, R. Rao, Jagannath, V. M. Naik, R. Naik, A. K. Tyagi, *Dalton Trans.* **2015**, *44*, 15872.
- [20] D. Mandal, K. Henkel, D. Schmeisser, *Mater. Lett.* **2012**, *73*, 123.
- [21] S. K. Ghosh, M. M. Alam, D. Mandal, *RSC Adv.* **2014**, *4*, 41886.
- [22] P. Martins, C. Caparros, R. Goncalves, P. M. Martins, M. Benelmekki, G. Botelho, S. Lanceros-Mendez, *J. Phys. Chem. C* **2012**, *116*, 15790.
- [23] S. Begum, A. Kausar, H. Ullah, M. Siddiq, *Polym.-Plast. Technol. Eng.* **2016**, *55*, 1949.
- [24] M. El Achaby, F. E. Arrakhiz, S. Vaudreuil, E. Essassi, A. Quaiss, M. Bousmina, *Polym. Eng. Sci.* **2013**, *53*, 34.
- [25] S. Manna, A. K. Nandi, *J. Phys. Chem. C* **2007**, *111*, 14670.
- [26] J. H. Lee, S. J. Kim, J. S. Park, J. H. Kim, *Macromol. Res.* **2016**, *24*, 909.
- [27] L. Hu, S. Dalgleish, M. M. Matsushita, H. Yoshikawa, K. Awaga, *Nat. Commun.* **2014**, *5*, 3279.
- [28] S. Jana, S. Garain, S. Sen, D. Mandal, *PCCP Phys. Chem. Chem. Phys.* **2015**, *17*, 17429.
- [29] H. X. Tang, Y. R. Lin, H. A. Sodano, *Adv. Energy Mater.* **2013**, *3*, 451.
- [30] Y. Feng, W. L. Li, Y. F. Hou, Y. Yu, W. P. Cao, T. D. Zhang, W. D. Fei, *J. Mater. Chem. C* **2015**, *3*, 1250.
- [31] X. Chen, H.-Y. Zhu, J.-C. Zhao, Z.-T. Zheng, X.-P. Gao, *Angew. Chem., Int. Ed.* **2008**, *47*, 5353.
- [32] X. G. Ding, C. H. Liow, M. X. Zhang, R. J. Huang, C. Y. Li, H. Shen, M. Y. Liu, Y. Zou, N. Gao, Z. J. Zhang, Y. G. Li, Q. B. Wang, S. Z. Li, J. Jiang, *J. Am. Chem. Soc.* **2014**, *136*, 15684.
- [33] L. Tong, Q. Wei, A. Wei, J.-X. Cheng, *Photochem. Photobiol.* **2009**, *85*, 21.
- [34] W. Park, D. Lu, S. Ahn, *Chem. Soc. Rev.* **2015**, *44*, 2940.
- [35] K. Aydin, V. E. Ferry, R. M. Briggs, H. A. Atwater, *Nat. Commun.* **2011**, *2*, 517.
- [36] M. Wang, M. Ye, J. Iocozzia, C. Lin, Z. Lin, *Adv. Sci.* **2016**, *3*, 1600024.
- [37] J. Hao, L. Zhou, M. Qiu, *Phys. Rev. B* **2011**, *83*, 165107.
- [38] Y. Hui, J. S. Gomez-Diaz, Z. Y. Qian, A. Alu, M. Rinaldi, *Nat. Commun.* **2016**, *7*, 11249.
- [39] A. C. Lopes, S. A. C. Carabineiro, M. F. R. Pereira, G. Botelho, S. Lanceros-Mendez, *ChemPhysChem* **2013**, *14*, 1926.
- [40] Z. G. Xiao, Q. F. Dong, P. Sharma, Y. B. Yuan, B. D. Mao, W. J. Tian, A. Gruverman, J. S. Huang, *Adv. Energy Mater.* **2013**, *3*, 1581.
- [41] T. P. Silverstein, *J. Chem. Educ.* **1998**, *75*, 116.
- [42] P. Martins, C. M. Costa, M. Benelmekki, G. Botelho, S. Lanceros-Mendez, *J. Mater. Sci.* **2013**, *48*, 2681.
- [43] P. Y. Xie, J. Wang, R. Tang, Z. M. Wu, Y. D. Jiang, *J. Mater. Sci. - Mater. Electron.* **2015**, *26*, 9067.
- [44] J. Gomes, J. S. Nunes, V. Sencadas, S. Lanceros-Mendez, *Smart Mater. Struct.* **2010**, *19*, 065010.
- [45] S. Bi, C. N. Sun, T. A. Zawodzinski, F. Ren, J. K. Keum, S. K. Ahn, D. W. Li, J. H. Chen, *J. Polym. Sci., Part B: Polym. Phys.* **2015**, *53*, 1450.
- [46] B. S. Ince-Gunduz, R. Alpern, D. Amare, J. Crawford, B. Dolan, S. Jones, R. Kobylarz, M. Reveley, P. Cebe, *Polymer* **2010**, *51*, 1485.
- [47] Q. P. Wang, S. L. Jiang, Y. Y. Zhang, G. Z. Zhang, L. Y. Xiong, *Polym. Bull.* **2011**, *66*, 821.
- [48] N. Maity, A. Mandal, A. K. Nandi, *Polymer* **2016**, *88*, 79.
- [49] I. Medina-Ramirez, S. Bashir, Z. P. Luo, J. L. Liu, *Colloids Surf., B* **2009**, *73*, 185.
- [50] A. C. Lopes, C. M. Costa, C. J. Tavares, I. C. Neves, S. Lanceros-Mendez, *J. Phys. Chem. C* **2011**, *115*, 18076.
- [51] S. Maji, P. K. Sarkar, L. Aggarwal, S. K. Ghosh, D. Mandal, G. Sheet, S. Acharya, *PCCP Phys. Chem. Chem. Phys.* **2015**, *17*, 8159.
- [52] L. You, N. T. Chua, K. Yao, L. Chen, J. L. Wang, *Phys. Rev. B* **2009**, *80*, 024105.
- [53] F. Yan, T. J. Zhu, M. O. Lai, L. Lu, *J. Appl. Phys.* **2011**, *110*, 084102.
- [54] Q. R. Lin, D. Y. Wang, Z. G. Chen, W. F. Liu, S. Lim, S. Li, *ACS Appl. Mater. Interfaces* **2015**, *7*, 26301.
- [55] T. A. Berfeld, R. J. Ong, D. A. Payne, N. R. Sottos, *J. Appl. Phys.* **2007**, *101*, 024102.
- [56] D. J. de Aberasturi, A. B. Serrano-Montes, L. M. Liz-Marzan, *Adv. Opt. Mater.* **2015**, *3*, 602.
- [57] S. Lincic, P. Christopher, D. B. Ingram, *Nat. Mater.* **2011**, *10*, 911.
- [58] K. L. Kelly, E. Coronado, L. L. Zhao, G. C. Schatz, *J. Phys. Chem. B* **2003**, *107*, 668.
- [59] P. Mulvaney, *Langmuir* **1996**, *12*, 788.
- [60] K. A. Willets, R. P. van Duyne, *Annu. Rev. Phys. Chem.* **2007**, *58*, 267.
- [61] L. Jiang, Y. X. Tang, C. H. Liow, J. S. Wu, Y. H. Sun, Y. Y. Jiang, Z. L. Dong, S. Z. Li, V. P. Dravid, X. D. Chen, *Small* **2013**, *9*, 705.
- [62] C. K. Sun, F. Vallee, L. H. Acioli, E. P. Ippen, J. G. Fujimoto, *Phys. Rev. B* **1994**, *50*, 15337.
- [63] N. Del Fatti, C. Voisin, M. Achermann, S. Tzortzakis, D. Christofilos, F. Vallee, *Phys. Rev. B* **2000**, *61*, 16956.
- [64] H. D. Young, R. A. Freedman, A. L. Ford, *Sears and Zeman-sky's University Physics: With Modern Physics*, Addison-Wesley, San Francisco, CA **2011**.
- [65] E. M. A. Fuentes-Fernandez, B. E. Gnade, M. A. Quevedo-Lopez, P. Shah, H. N. Alshareef, *J. Mater. Chem. A* **2015**, *3*, 9837.